energies

MDPI

Article

Enhancing the Structural and Electrochemical Properties of Lithium Iron Phosphate via Titanium Doping During Precursor Synthesis

Puliang Li [1,2], Yang Wang [1,2], Weifang Liu [3], Tao Chen [1,2] and Kaiyu Liu [1,2,*]

[1] College of Chemistry and Chemical Engineering, Central South University, Changsha 410083, China; lpl79@163.com (P.L.); 242311110@csu.edu.cn (Y.W.); taochen4486@163.com (T.C.)
[2] Hunan Provincial Key Laboratory of Chemical Power Sources, College of Chemistry and Chemical Engineering, Central South University, Changsha 410083, China
[3] College of Chemistry and Chemical Engineering, Hunan University of Science & Technology, Xiangtan 410082, China; 1060161@hnust.edu.cn
* Correspondence: kaiyuliu309@163.com

Abstract: This study investigates the effects of different titanium doping concentrations on the properties of iron phosphate precursors and the final lithium iron phosphate ($LiFePO_4$) materials, aiming to optimize the structural and electrochemical performance of $LiFePO_4$ by introducing titanium during the precursor synthesis stage. Titanium was introduced using titanate as a titanium source to prepare iron phosphate precursors with varying titanium concentrations. The materials were characterized using X-ray diffraction (XRD), scanning electron microscopy (SEM), and other techniques. The results showed that titanium incorporation significantly influenced the Fe and P content in the precursors, with a decrease in both Fe and P levels as the titanium doping concentration increased. Moreover, as the titanium content increased, the particle size of the precursor decreased, and the particle distribution became more uniform. Additionally, titanium doping improved the tap density of the precursors, with a significant increase in tap density observed when the titanium content reached 4000 ppm. Electrochemical measurements revealed that titanium doping had a certain impact on the discharge capacity of $LiFePO_4$, with the discharge capacity gradually decreasing as the titanium content increased. Overall, this study effectively improved the physical properties of $LiFePO_4$ materials by introducing titanium during the precursor synthesis stage, providing a theoretical foundation for further optimization of titanium-doped $LiFePO_4$.

Keywords: titanium doping; lithium iron phosphate; iron phosphate precursor; lithium-ion batteries

check for updates

Received: 1 January 2025
Revised: 10 February 2025
Accepted: 13 February 2025
Published: 14 February 2025

Citation: Li, P.; Wang, Y.; Liu, W.; Chen, T.; Liu, K. Enhancing the Structural and Electrochemical Properties of Lithium Iron Phosphate via Titanium Doping During Precursor Synthesis. *Energies* **2025**, *18*, 930. https://doi.org/10.3390/en18040930

Copyright: © 2025 by the authors. Licensee MDPI, Basel, Switzerland. This article is an open access article distributed under the terms and conditions of the Creative Commons Attribution (CC BY) license (https://creativecommons.org/licenses/by/4.0/).

1. Introduction

The rapid development of electric vehicles (EVs) and renewable energy storage systems has significantly increased the demand for high-performance lithium-ion batteries (LIBs) [1,2]. As one of the most promising energy storage technologies, LIBs offer high energy density, long cycle life, and relatively fast charging capabilities [3,4]. Among various types of cathode materials, lithium iron phosphate ($LiFePO_4$) has gained considerable attention for its excellent safety, thermal stability, and low cost [5]. Its robust electrochemical performance, long cycle life, and environmental friendliness make it particularly suitable for large-scale applications in EVs and stationary energy storage [6–8]. However, $LiFePO_4$'s

relatively low electrical conductivity and poor tap density limit its performance in high power density and long-term cycling stability [9–11].

To address these limitations, various strategies have been employed to enhance the properties of $LiFePO_4$ [12,13]. One of the most commonly used methods is doping with transition metals, which can improve the conductivity, stability, and density of the material [14,15]. Among these, titanium (Ti) doping has been shown to be highly effective in enhancing the structural stability and electronic conductivity of $LiFePO_4$ by altering its electronic structure [16,17]. Titanium doping not only helps improve the rate capability and cycling performance but also contributes to the enhancement of the material's tap density [18,19]. However, conventional Ti doping methods—such as physically mixing titanium dioxide (TiO_2) with $LiFePO_4$ precursors followed by high-temperature sintering—often lead to uneven distribution of titanium within the material. This non-uniform distribution of Ti can result in suboptimal performance of the final product, as Ti is not always well-incorporated into the lattice structure of $LiFePO_4$ [20].

In recent years, attention has been drawn titanium directly during the precursor synthesis stage [21]. This approach ensures a more uniform distribution of titanium throughout the material and improves the overall performance of the final product. Incorporating Ti at the precursor stage has been found to better control the doping level and achieve more consistent material properties [22]. By adding titanium during the synthesis of iron phosphate precursors, a more stable and homogeneous Ti distribution can be achieved, which is critical for improving both the structural and electrochemical properties of $LiFePO_4$ [23–25]. This method has been recognized as a promising strategy for enhancing the performance of titanium-doped $LiFePO_4$ materials [26–28].

This work aims to explore the use of titanate as a titanium source in the synthesis of iron phosphate and systematically investigate the effects of different Ti doping levels on the properties of both the iron phosphate precursor and the final $LiFePO_4$ product. Specifically, this study will focus on how varying Ti concentrations influence the structural, morphological, and electrochemical properties of the materials, with the goal of providing new insights into improving the performance of $LiFePO_4$ cathode materials. The research will also examine the role of titanium during the precursor synthesis stage and evaluate its impact on particle size, density, and electrochemical behavior, offering new theoretical and technical approaches for the development of high-performance lithium-ion batteries.

2. Experimental

2.1. Material Synthesis

2.1.1. Preparation of Ferrous Sulfate Solution

Ferrous sulfate (Beijing Chemicals Co., Beijing, China) and deionized water (School of Chemistry and Chemical Engineering, Central South University, Changsha, China) are added to a reaction vessel in a 1:1 ratio. The mixture is then heated to 50–60 °C, ensuring complete dissolution. Ammonia solution (Guangzhou Chemical Reagent Factory, Guangzhou, China) is subsequently added to adjust the pH to 4.5–5, followed by filtration. Sulfuric acid (Wuxi Chemical Plant, Wuxi, China) is introduced to adjust the pH to 1.5–1.8, and the solution is filtered again. The solution is then diluted with deionized water to achieve a final ferrous sulfate concentration of 70–71 g/L. The prepared solution is sealed and stored for later use.

2.1.2. Preparation of Ammonium Dihydrogen Phosphate Solution

Ammonium dihydrogen phosphate (Beijing Chemicals Co., Beijing, China) is dissolved in deionized water at a 1:5 ratio, and the mixture is heated to 40–50 °C while stirring until fully dissolved. The solution is then filtered to obtain the filtrate. Deionized water is added

to the filtrate to adjust the phosphate concentration to 45–47 g/L. The solution is sealed and stored for later use.

2.1.3. Preparation of Titanium-Doped Iron Phosphate with Different Titanium Concentrations

A total of 1 L of ferrous sulfate solution is transferred into a glass flask. Then, different concentrations of titanate solutions (prepared by dissolving 1.25, 2.5, 3.75, 5, 6.25, and 7.5 g of titanate in 1 L of water) are added to the ferrous sulfate solution. The flask is placed in a constant-temperature water bath, and the temperature is increased to 60 °C and maintained. Next, an ammonium dihydrogen phosphate solution is added according to a P:Fe molar ratio of 1.06. Hydrogen peroxide, 1.5 times the total iron amount, is then added and stirred thoroughly. Deionized water is added to adjust the volume to 1 L. Stirring is initiated at 500 rpm, and the phosphate solution is slowly added to the ferrous sulfate solution over a period of 100 min. After the phosphate salt is fully added, the temperature of the water bath is increased to 92 °C and maintained until the material turns white. The white slurry is then filtered and washed until the conductivity is below 500 μS/cm. Afterward, pure water is added to the slurry at a solid content of 20%, and 85% phosphoric acid (Yancheng Chemical Reagents Co., Yancheng, China) is added. The slurry is then transferred to a glass flask, placed in a constant-temperature water bath, and heated to 92 °C while stirring at 500 rpm for 2 h. After the reaction, the mixture is filtered and washed until the conductivity of the wash water is below 200 μS/cm. The washed filter cake is placed in an oven and dried at 105 °C for 12 h to obtain dihydrate iron phosphate. The obtained dihydrate iron phosphate is then sintered in a muffle furnace (Zhengzhou Lab Equipment Co., Zhengzhou, China) at 560 °C for 4 h to produce anhydrous iron phosphate with varying titanium doping levels, which are referred to as TFP-1, TFP-2, TFP-3, TFP-4, TFP-5, and TFP-6, respectively.

2.1.4. Preparation of Titanium-Doped Lithium Iron Phosphate

Lithium iron phosphate (Jiangxi Special Electric Motor Co., Nanchang, China) and lithium carbonate (Ganfeng Lithium Co., Xinyu, China) are weighed according to a Li:Fe molar ratio of 1.04. Additionally, glucose (Shandong Pharmaceutical Industry Co., Jinan, China), accounting for 10% of the total weight of lithium iron phosphate and lithium carbonate, is weighed and added to the mixture. The materials are then placed in a grinding cup and deionized water is added to achieve a solid content of 45%. The mixture is ground until the D50 particle size is 0.35–0.4 μm. The dried material is transferred to a quartz crucible and then placed in a tube furnace (Zhengzhou Lab Equipment Co., Zhengzhou, China. Under nitrogen protection, the material is sintered at 740 °C for 8 h to produce the lithium iron phosphate cathode materials, referred to as LTFP-1, LTFP-2, LTFP-3, LTFP-4, LTFP-5, and LTFP-6, respectively.

2.2. Materials Characterization

The tapped density of the material was measured using a BT-310 powder tapping density tester (Guangdong Fuke Instrument Co., Guangzhou, China). Particle size analysis was conducted with a laser diffraction particle size analyzer (Malvern Instruments, Malvern, UK). X-ray diffraction patterns were acquired using a Bruker Advance-D8 diffractometer (Bruker, Karlsruhe, Germany), employing Cu Kα radiation as the source. The analysis of metal element content was performed via inductively coupled plasma atomic emission spectrometry (ICP-AES) (PerkinElmer, Waltham, MA, USA). Additionally, the morphologies of the materials were observed through scanning electron microscopy (SEM) images, utilizing a FEI Nova Nano SEM 230 instrument (Thermo Fisher Scientific, Hillsboro, OR, USA).

2.3. Electrochemical Measurements

To investigate the electrochemical properties of the fabricated cathode materials, coin-type (CR2032) cells were assembled in an argon-filled glove box (MBraun, Garching, Germany). All of the electrochemical tests were measured in a standard CR2032-type coin (Guangdong Canrd New Energy Technology Co., Ltd., Guangdong, China) cell at room temperature (25 °C). The composite electrodes were prepared by the active material, acetylene black ((Alfa Aesar, Haverhill, MA, USA), and polyvinylidene fluoride (PVDF, Sigma-Aldrich, St. Louis, MO, USA) with a weight ratio of 8:1:1 to disperse in 1-methyl-2-pyrrolidinone (NMP). The slurry was uniformly coated on the aluminum (Alcoa, Pittsburgh, PA, USA). The prepared electrodes were then dried in a vacuum oven (Thermo Fisher Scientific, Waltham, MA, USA) at 80 °C for 24 h. The mass loading of the active materials ranged from 1.5 to 2 mg/cm^2. All cells were assembled using a pure lithium foil (Ferro, Independence, OH, USA) as the negative electrode and glass fiber (Whatman, GF/D, Maidstone, UK) as the separator in a glove box which was filled with argon. The electrolyte was prepared using diethyl carbonate (DEC, AR, Sinopharm, Beijing, China) and ethylene carbonate (EC, AR, Sinopharm, Beijing, China) (using a volume ratio of 1:1) as solvent, which dissolved into 1 M LiPF6 (AR, Sinopharm, Beijing, China) as solute. The obtained CR2032 coin-type cells were charged at 0.1 C at 25 °C between 2.5 and 4.2 V (vs. Li/Li$^+$) on a NEWARE battery test system (Neware Technology, Shenzhen, China), and the 1 C rate was 170 mA g^{-1}.

3. Results and Discussion

Based on the data in Table 1, the Ti content of the product has reached the design target, with deviations within an acceptable range. This indicates that the synthesis method we employed is effective in introducing a quantifiable amount of Ti into the iron phosphate precursor. In addition, as shown in Figure 1, the doping of Ti significantly influences the Fe and P content in the iron phosphate precursor. Upon the incorporation of Ti into the iron phosphate, both Fe and P contents decrease simultaneously, and the reduction in Fe and P levels becomes more pronounced as the Ti doping concentration increases. This concurrent decrease in Fe and P content suggests that Ti may exist in the product primarily in the form of an oxide, rather than disrupting the overall structure of the iron phosphate. This implies that the Ti doping does not compromise the structural integrity of the precursor. When the iron phosphate is later converted into lithium iron phosphate ($LiFePO_4$), this structural preservation of the precursor can be beneficial for optimizing the electrochemical performance of the final product.

Figure 2 shows the relationship between the tapped density of iron phosphate and the titanium (Ti) content in the samples. The data indicate that the introduction of Ti into iron phosphate affects its tapped density. Specifically, the addition of Ti enhances the tapped density. For the TFP-5 sample, the tapped density significantly increased to 0.74, whereas the tapped densities of the TFP-1, TFP-2, and TFP-3 gradient samples were around 0.6. When the Ti content reaches 4000 ppm, further increases in Ti content do not lead to additional improvements in tapped density. In the sample with the highest Ti content, TFP-6, the tapped density did not increase further. This suggests that the amount of Ti introduced needs to be controlled within a certain range to achieve the optimal tapped density.

Figure 3 illustrates the relationship between the titanium (Ti) content and the particle size of the precursor products. It can be observed that the TFP-1 product, with the lowest Ti content, has a D50 of 8.97 μm and a D100 of 76.787 μm. In contrast, the TFP-6 product, with the highest Ti content, shows a D50 of 3.07 μm and a D100 of 14.629 μm. This indicates that as the Ti content increases, the particle size of the iron phosphate precursor product decreases.

Table 1. The chemical composition and physical properties of iron phosphate precursors with different Ti doping levels.

Sample		TFP-1	TFP-2	TFP-3	TFP-4	TFP-5	TFP-6
Fe %		36.25	36.26	36.24	36.21	36.20	36.18
P %		20.86	20.8	20.76	20.66	20.67	20.65
Fe/P		0.9638	0.9668	0.9681	0.9720	0.9711	0.9717
Ti ppm		948.4	2560	3599	4589	5409	6740
S ppm		136	109	81	187	81	96
specific surface area (m^2/g)		5.661	6.836	6.759	5.527	5.265	6.389
tap density (g/cm^3)		0.58	0.57	0.64	0.73	0.74	0.72
pH		3.29	3.02	2.94	3.02	3.23	3.3
particle size (um)	D50	8.97%	6.58%	4.567%	3.945%	2.7%	3.07%
	D100	76.787%	76.007%	57.366%	23.48%	17.69%	14.629%
impurity element (ppm)	Al	1.35	3.106	3.154	1.573	2.266	1.94
	Ca	4.459	2.859	3.538	16.35	17.36	25.17
	Cr	15.71	17.16	15.07	17.77	13.47	15.89
	Cu	0	0	0	0	0	0.717
	Na	3.962	0	0	0	0	5.673
	K	21.22	16.91	14.58	4.601	3.954	19.01
	Pb	9.692	11.42	9.002	10.88	9.237	11.09

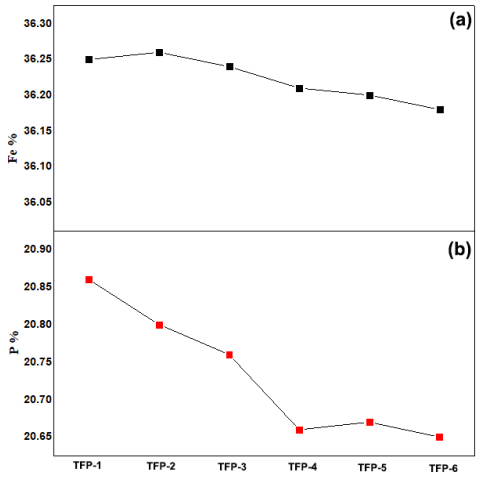


Figure 1. Variation in the (**a**) Fe and (**b**) P content in samples with different Ti doping levels.

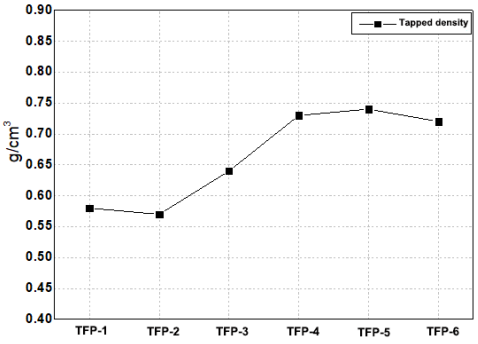


Figure 2. Variation in the tapped density of iron phosphate precursor samples with different Ti doping levels.

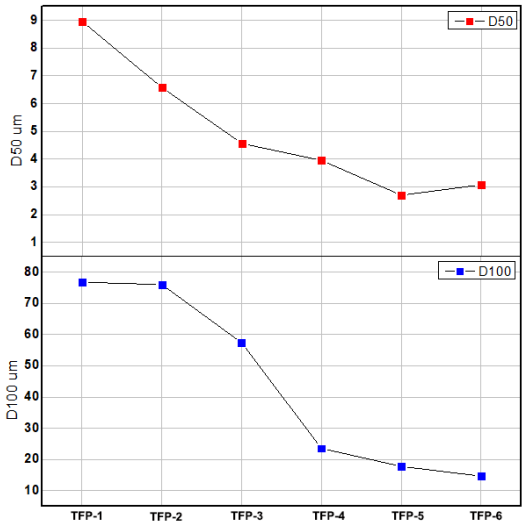


Figure 3. Distribution of particle size percentages at D50 and D100 for iron phosphate precursor samples with different Ti doping levels.

Figure 4 presents the scanning electron microscope (SEM) images of iron phosphate precursors with different Ti doping levels. In the TFP-1 sample, the particles are relatively uniform. However, in the TFP-4, TFP-5, and TFP-6 samples, which have higher Ti doping levels, larger iron phosphate particles are observed, forming a particle size distribution with both small and large particles, along with more agglomerates. The smaller particles seem to fill the gaps between the larger particles, which may explain why the tapped density of iron phosphate increases with higher Ti content.

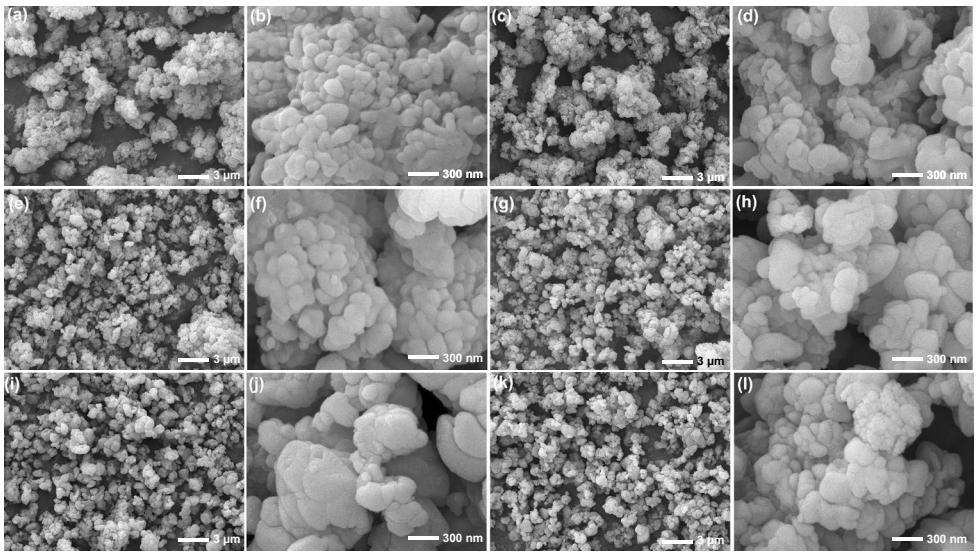


Figure 4. SEM images of (**a**,**b**) TFP-1, (**c**,**d**) TFP-2, (**e**,**f**) TFP-3, (**g**,**h**) TFP-4, (**i**,**j**) TFP-5, and (**k**,**l**) TFP-6 samples.

Figure 5 shows the XRD spectra of iron phosphate and lithium iron phosphate with different titanium (Ti) doping levels. From the spectra, it can be seen that the Ti-doped iron phosphate samples and lithium iron phosphate all match the standard card 29-0715 and 40-1499 [29,30], respectively. Furthermore, as the Ti doping amount increases, no new impurity peaks appear, indicating that the resulting Ti-doped iron phosphate is a single-phase material. This also suggests that Ti has been successfully incorporated into the crystal structure of $FePO_4$ and $LiFePO_4$.

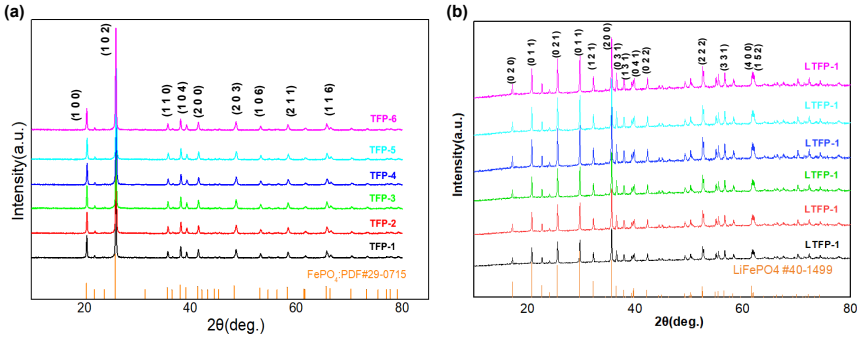


Figure 5. XRD spectra of (**a**) iron phosphate precursors and (**b**) lithium iron phosphate with different Ti contents.

$LiFePO_4$ cathode materials were prepared using iron phosphate doped with different Ti contents as the raw material. As shown in Figure 6, the method of doping titanium not only results in a more uniform distribution of Ti in $LiFePO_4$ compared to other studies [31,32], but the doping level of Ti also has a significant impact on the morphology of $LiFePO_4$. From the morphology, it can be observed that the particles are agglomerates with a near-spherical shape. Furthermore, as the Ti content increases, the proportion of larger particles significantly increases. This suggests that Ti doping promotes the growth of $LiFePO_4$ particles, which is beneficial for forming a particle size distribution with both small and large particles, contributing to an improved tapped density. To verify this, the tapped density of $LiFePO_4$ with different titanium (Ti) contents was measured, as shown in Figure 7. As the Ti content increases, the tapped density of $LiFePO_4$ is effectively enhanced. However, when the Ti content reaches LTFP-4, the tapped density levels off and no longer increases further.

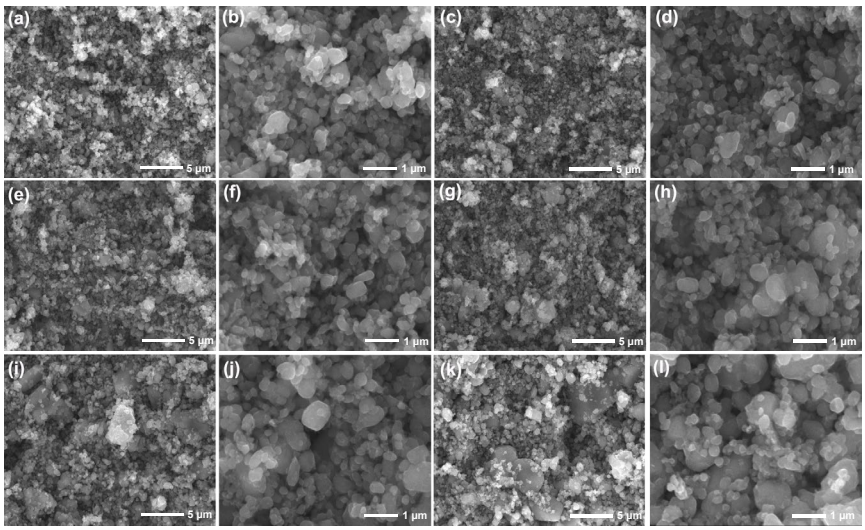


Figure 6. SEM images of (**a**,**b**) LTFP-1, (**c**,**d**) LTFP-2, (**e**,**f**) LTFP-3, (**g**,**h**) LTFP-4, (**i**,**j**) LTFP-5, and (**k**,**l**) LTFP-6 samples.

Figure 8a shows the 0.1 C discharge capacity curves of $LiFePO_4$ with different titanium (Ti) doping levels. For the LTFP-1 sample, the 0.1 C specific capacity is the highest at 161.31 mAh/g. As the Ti doping level increases, the discharge capacity of $LiFePO_4$ gradually decreases. For the LTFP-4 sample, the 0.1 C specific capacity is 159.42 mAh/g, while for the LTFP-6 sample, the 0.1 C specific capacity is the lowest at 157.28 mAh/g. The cycling stability test for LTFP-1 is shown in Figure 8b. The initial discharge specific capacity at 1 C is 149.73 mAh/g, and after stable cycling for 150 cycles, the capacity retention rate reaches 89.54%. This indicates that the cathode material prepared by this method exhibits good cycling stability.

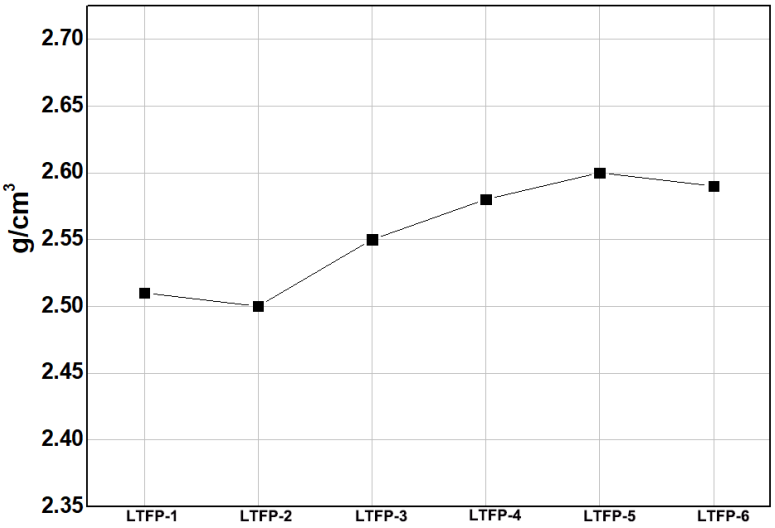


Figure 7. Variation in the tapped density of lithium iron phosphate samples with different Ti doping levels.

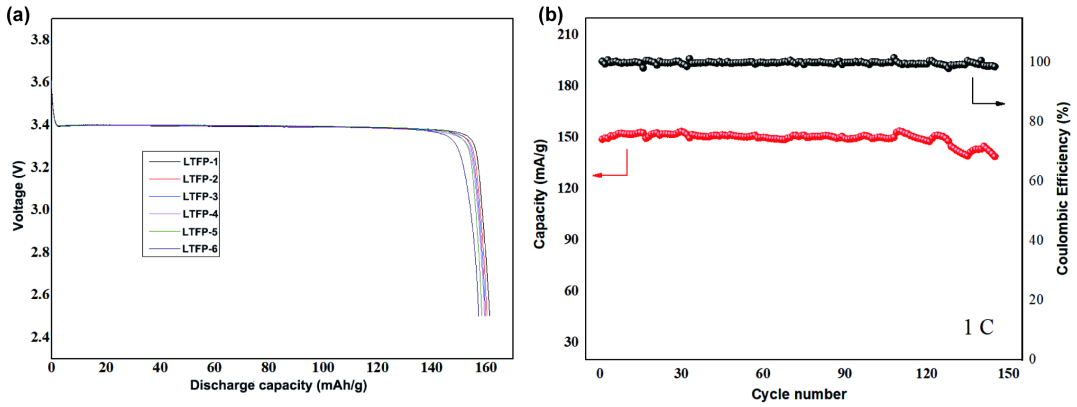


Figure 8. (**a**) The discharge capacity of lithium iron phosphate samples with different Ti doping levels; (**b**) the cycling performance of LTFP-1 at 1 C.

4. Conclusions

This study systematically investigates the effects of titanium (Ti) doping on the structural, morphological, and electrochemical properties of $LiFePO_4$. The results show that Ti doping improves the tapped density and particle morphology, with optimal enhancement observed at LTFP-4. As Ti content increases, the particles grow larger, leading to a more favorable particle size distribution. However, beyond a certain Ti concentration, specifically at 5000 ppm and above, the discharge capacity starts to decrease, indicating a trade-off between structural enhancement and electrochemical performance. These findings provide important insights into the role of Ti doping in optimizing the performance of $LiFePO_4$ cathodes, offering a balance between improved material properties and maintained electrochemical efficiency for high-performance lithium-ion batteries.

Author Contributions: Conceptualization, P.L.; Methodology, P.L.; Software, P.L.; Validation, P.L.; Formal analysis, P.L.; Data curation, P.L.; Writing—original draft, P.L.; Writing—review and editing, Y.W. and T.C.; Visualization, P.L. and K.L.; Supervision, W.L. and K.L.; Project administration, W.L. and K.L. All authors have read and agreed to the published version of the manuscript.

Funding: This research was funded by the National Natural Science Foundation of China (No. 22272204) and the Hunan Provincial Natural Science Foundation Project (No. 2023JJ40276).

Data Availability Statement: The original contributions presented in the study are included in the article; further inquiries can be directed to the corresponding author.

Conflicts of Interest: The authors declare no conflicts of interest.

References

1. Cao, Z.; Ma, B.; Jing, Q.; Xing, P.; Liu, B.; Wang, C. Facile and inexpensive preparation method of iron phosphate from laterite residue. *Ceram. Int.* **2020**, *46*, 11304–11310. [CrossRef]
2. Yang, S.; Zavalij, P.Y.; Whittingham, M.S. Stanley Whittingham. Hydrothermal synthesis of lithium iron phosphate cathodes. *Electrochem. Commun.* **2001**, *3*, 505–508. [CrossRef]
3. Sugiyama, S.; Ichii, T.; Fujisawa, M.; Kawashiro, K.; Tomida, T.; Shigemoto, N.; Hayashi, H. Heavy metal immobilization in aqueous solution using calcium phosphate and calcium hydrogen phosphates. *J. Colloid Interface Sci.* **2003**, *259*, 408–410. [CrossRef] [PubMed]
4. Zhou, W.; He, W.; Wang, M.; Zhang, X.; Li, P.; Yan, S.; Tian, X.; Sun, X.; Han, X. Biosynthesis and characterization of layered iron phosphate. *Smart Mater. Struct.* **2008**, *17*, 065034. [CrossRef]
5. Syutkin, S.A.; Pervushin, V.Y.; Kuznetsov, G.F.; Kleshchev, D.G.; Zherebtsov, D.A.; German, V.A.; Viktorov, V.V.; Kolmogorov, A.M.; Serikov, A.S. Transformations of hydrated titanium dioxide in hydrothermal treatment. *Russ. J. Appl. Chem.* **2010**, *83*, 1209–1214. [CrossRef]
6. Davidson, M.; Ngo, C.; Gage, S.H.; Pylypenko, S.; Trewyn, B.G. Direct synthesis of Fe rich SBA-15 at low pH by in-situ formation of iron phosphate phase. *Microporous Mesoporous Mater.* **2019**, *276*, 270–279. [CrossRef]
7. Dean, J.A. Lange's Handbook of Chemistry. *Mater. Manuf. Process.* **1990**, *5*, 687–688. [CrossRef]
8. Deng, L.; Ma, G.; Chen, Q. Preparation of Iron Phosphate Battery Materials from Industrial Ferrous Sulfate Waste by Liquid Phase Method. *Integr. Ferroelectr.* **2023**, *234*, 67–78. [CrossRef]
9. Barbara, G.; Daniel, G.; Bogumi, K. Effects of processing parameters on hydrolysis of $TiOSO_4$. *Pol. J. Chem. Technol.* **2009**, *11*, 15–21.
10. Hsieh, C.-T.; Chen, I.L.; Chen, W.-Y.; Wang, J.-P. Synthesis of iron phosphate powders by chemical precipitation route for high-power lithium iron phosphate cathodes. *Electrochim. Acta* **2012**, *83*, 202–208. [CrossRef]
11. Jiang, T.; Tu, Y.; Su, Z.; Lu, M.; Liu, S.; Liu, J.; Gu, F.; Zhang, Y. A novel value-added utilization process for pyrite cinder: Selective recovery of Cu/Co and synthesis of iron phosphate. *Hydrometallurgy* **2020**, *193*, 105314. [CrossRef]
12. Jiang, Y.; Zhang, G.; Zhou, K.; Peng, C.; Salih, K.A.M.; Zhou, H.; Wu, Y.; Chen, W. Sequential separation and recovery of phosphorus and lithium from lithium phosphate slag by selective extraction-precipitation. *Sep. Purif.* **2024**, *333*, 125907. [CrossRef]
13. Kim, J.; Li, W.; Philips, B.L.; Grey, C.P. Phosphate adsorption on the iron oxyhydroxides goethite (α-FeOOH), akaganeite (β-FeOOH), and lepidocrocite (γ-FeOOH): A 31P NMR Study. *Energy Environ. Sci.* **2011**, *4*, 4298–4305. [CrossRef]
14. Lou, W.-B.; Zhang, Y.; Zhang, Y.; Zheng, S.-L.; Sun, P.; Wang, X.-J.; Li, J.-Z.; Qiao, S.; Zhang, Y.; Wenzel, M.; et al. Leaching performance of Al-bearing spent $LiFePO_4$ cathode powder in H_2SO_4 aqueous solution. *Trans. Nonferrous Met. Soc.* **2021**, *31*, 817–831. [CrossRef]
15. Jin, J.; Liu, X.; Yuan, S.; Gao, P.; Li, Y.; Zhang, H.; Meng, X. Innovative utilization of red mud through co-roasting with coal gangue for separation of iron and aluminum minerals. *J. Ind. Eng. Chem.* **2021**, *98*, 298–307. [CrossRef]
16. Jiang, Y.; Peng, C.; Zhou, K.; Hu, Z.; Zhang, G.; Wu, Y.; Zhang, J.; Chen, W. Recovery of iron from titanium white waste for the preparation of $LiFePO_4$ battery. *J. Clean. Prod.* **2023**, *415*, 137817. [CrossRef]
17. Zhang, W.; Zhang, T.-A.; Cai, L.; Lv, G.; Cao, X. Preparation of Doped Iron Phosphate by Selective Precipitation of Iron from Titanium Dioxide Waste Acid. *Metals* **2020**, *10*, 789. [CrossRef]
18. Zherebtsov, D.A.; Syutkin, S.A.; Pervushin, V.Y.; Kuznetsov, G.F.; Kleshchev, D.G.; German, V.A.; Viktorov, V.V.; Kolmogortsev, A.M.; Serikov, A.S. Characteristics of the hydrous titanium dioxide-anatase phase transformation during hydrothermal treatment in aqueous solutions. *Russ. J. Inorg. Chem.* **2010**, *55*, 1197–1201. [CrossRef]
19. Zhu, Y.-M.; Ruan, Z.-W.; Tang, S.-Z.; Thangadurai, V. Research status in preparation of $FePO_4$: A review. *Ionics* **2014**, *20*, 1501–1510. [CrossRef]
20. Lundager Madsen, H.E.; Koch, C.B. Kinetics of solution crystal growth of strengite, $FePO_4$,$2H_2O$. *J. Cryst. Growth* **2018**, *482*, 9–14. [CrossRef]
21. Xiao, C.; Xiao, L.; Gao, C.; Zeng, L. Thermodynamic study on removal of magnesium from lithium chloride solutions using phosphate precipitation method. *Sep. Purif.* **2015**, *156*, 582–587. [CrossRef]
22. He, L.; Xu, W.; Song, Y.; Liu, X.; Zhao, Z. Selective removal of magnesium from a lithium-concentrated anolyte by magnesium ammonium phosphate precipitation. *Sep. Purif.* **2017**, *187*, 214–220. [CrossRef]

23. Kumar, N.; Bhardwaj, N.K.; Chakrabarti, S.K.; Kumar, S. Synthesis and application of calcium sulphate pigment for paper coating: Potential and prospects. *Powder Technol.* **2012**, *218*, 40–45. [CrossRef]
24. Liu, Y.; Wang, J.; Liu, J.; Banis, M.N.; Xiao, B.; Lushington, A.; Xiao, W.; Li, R.; Sham, T.-K.; Liang, G.; et al. Origin of phase inhomogeneity in lithium iron phosphate during carbon coating. *Nano Energy* **2018**, *45*, 52–60. [CrossRef]
25. Zhao, C.X.; Liu, J.N.; Li, B.Q.; Ren, D.; Chen, X.; Yu, J.; Zhang, Q. Multiscale Construction of Bifunctional Electrocatalysts for Long-Lifespan Rechargeable Zinc–Air Batteries. *Adv. Funct.* **2020**, *30*, 2003619. [CrossRef]
26. Xiao, C.; Zeng, L.; Wei, J.; Xiao, L.; Zhang, G. Thermodynamic analysis for the separation of tungsten and aluminium in alkaline medium using solvent extraction. *Hydrometallurgy* **2017**, *174*, 91–96. [CrossRef]
27. Zou, W.; Feng, X.; Wang, R.; Wei, W.; Luo, S.; Zheng, R.; Yang, D.; Mi, H.; Chen, H. High-efficiency core-shell magnetic heavy-metal absorbents derived from spent-$LiFePO_4$ Battery. *J. Hazard. Mater.* **2021**, *402*, 123583. [CrossRef]
28. Chen, T.; Qiu, C.; Zhang, X.; Wang, H.; Song, J.; Zhang, K.; Yang, T.; Zuo, Y.; Yang, Y.; Gao, C.; et al. An Ultrasmall Ordered High-Entropy Intermetallic with Multiple Active Sites for the Oxygen Reduction Reaction. *J. Am. Chem. Soc.* **2023**, *146*, 1174–1184. [CrossRef]
29. *PDF#29-0715*; Iron Phosphate. International Center for Diffraction Data: Newtown Square, PA, USA, 2016.
30. *PDF#40-1499*; Lithium Iron Phosphate. International Center for Diffraction Data: Newtown Square, PA, USA, 2016.
31. Zhang, C.; Liang, Y.; Yao, L.; Qiu, Y. Synthesis and characterization of $LiFePO_4$-carbon nanofiber with Ti4+ substitution by electrospinning and thermal treatment. *Solid State Ionics* **2014**, *267*, 74–79. [CrossRef]
32. Li, L.; Li, X.; Wang, Z.; Wu, L.; Zheng, J.; Guo, H. Stable cycle-life properties of Ti-doped $LiFePO_4$ compounds synthesized by co-precipitation and normal temperature reduction method. *J. Phys. Chem. Solids* **2009**, *70*, 238–242. [CrossRef]

Disclaimer/Publisher's Note: The statements, opinions and data contained in all publications are solely those of the individual author(s) and contributor(s) and not of MDPI and/or the editor(s). MDPI and/or the editor(s) disclaim responsibility for any injury to people or property resulting from any ideas, methods, instructions or products referred to in the content.